LAWRENCE
LIVERMORE
NATIONAL
LABORATORY

LLNL-CONF-452912

Silica Molecular Dynamic Force Fields- A Practical Assessment

T, Soules, G. H. Gilmer, M. J. Matthews, J. S. Stolken, M. D. Feit

September 2, 2010

SPIE 2010
Boulder , CO, United States
September 26, 2010 through September 29, 2010

Disclaimer

Silica Molecular Dynamic Force Fields - a Practical Assessment

Thomas F. Soules, George H. Gilmer, Manyalibo J. Matthews, James S. Stolken and Michael D. Feit

National Ignition Facility and Photon Sciences, Lawrence Livermore National Laboratory

7000 East Avenue, Livermore, California 94550

(Received)

Abstract

The purpose of this paper is to compare simple and efficient pairwise force fields for silica glass and assess their applicability for use in large scale molecular dynamic (MD) simulations of laser damage mitigation. Pairwise potentials obtained by fitting quantum mechanical results, such as the BKS and CHIK potentials exhibit many of the properties of the liquid such as densification. However while this and other liquid properties of the MD simulation are qualitatively correct they are observed at temperatures much higher than observed experimentally. Softer potentials are constructed that do give liquid properties at experimental temperatures. However in all cases the activation energies for diffusion are lower than the activation energies for viscosity.

I. INTRODUCTION

In the National Ignition Facility at Lawrence Livermore National Laboratory surface damage to silica optics caused by the high intensities of lasers used to induce fusion is currently being mitigated by pulsed CO_2 laser treatments. The mitigating laser pulses can raise a small silica damage site to temperatures of 2000 - 5000 K in 10^{-9} to 10^{-12} s. This causes the damaged site to 'heal' or at least change its optical

properties so that light traveling through does not cause further damage. Evaporation and ablation can also be induced depending on the power and temporal shape of the pulses. The effects of these laser mitigation pulses are being modeled with finite-element tools[1]. However fundamental properties of silica, such as, heat capacities, thermal conductivities, thermal expansion, etc. during the very rapid heating and cooling of silica to very high temperatures are frequently unknown and cannot be obtained independently experimentally. MD simulations performed with simple potentials that faithfully reproduce experimental data under less severe conditions could be a practical tool for obtaining these properties and even simulating the mitigation experiment[2]. Conversely the laser experimental results can probe the silica glass and liquid under conditions not previously accessible.

Our initial objective was to simulate the laser mitigation using MD and the force fields developed by van Beest, Kramer and van Santen (BKS)[3] who fit self-consistent-field (SCF) Hartree-Fock calculations on small silica molecules. The BKS potential has impressively been shown to reproduce at least the features of the complicated phase diagram of SiO_2 including qualitatively the regions of stability of the liquid, stishovite, coesite and β-quartz phases.[4] On the other hand a BKS MD model of β-crystobalite homogenously melts at ~5000 ^{o}K in the MD (NPT) heating versus the experimental thermodynamic melting temperature ~2000 ^{o}K and boiling point ~ 3000 ^{o}K. The periodic boundary constraints of the MD simulation, its rapid heating rate and the absence of any nucleating site are no doubt responsible for failure of the structure to melt at a lower temperature. However, Saiko-Voivod, et al.[4] estimate a thermodynamic melting point for β-quartz by finding the point where the free energy is equal to that of the liquid at near atmospheric temperature to be ~ 3700 K . Further altough the

[1] M. J. Matthews, J. S. Stolken, R. M. Vignes, M. A. Norton, S. Yang, J. D. Cooke, G. M Guss, and J. J. Adams, Proc. of SPIE 7504, 750410 (2009); T. D. Bennett and Lei Li, J. Appl. Physics, 89, 942-950 (2001); J. Appl. Physics, 95, 5476-5482 (2004).
[2] As an example of a large scale silica MD simulation see - A. Kubota, M. –J. Caturla, S.A. Payne, T. Diaz de la Rubia and J. F. Latkowski, J. Nuc. Mat. 307, 891-894 (2002).
[3] B. W. H. van Beest, G. J. Kramer, and R. A. van Santen, Phys. Rev. Lett. **64**, 1955 (1990).
[4] I. Saiko-Voivod, F. Sciortino, T. Grande and P. H. Poole, Phys. Rev. E **70,** 061507 (2004).

equilibrium BKS silica liquid shows a density maximum similar the real liquid silica[5] and other liquids having a random tetrahedral network, this maximum occurs at ~4700 ^{o}K versus the experimental vitreous silica density increase at 1820 ^{o}K [6]. Hence it seems prudent to assess the behavior of vitreous silica simulations versus experiment with different simple force fields before constructing large scale MD ensembles that purport to model the behavior of real silica optic damage sites under laser mitigation.

Because of its importance in many fields from geophysical science to photonics and its role as the archetypical strong glass former[7] there have been many MD simulations of silica with different force fields. They fall roughly into three groups: The first simulations of silica by Woodcock, Cheeseman and Angell (WCA)[8] used a simple Born-Mayer (BM) potential with ionic charges of +4 for Si and -2 for oxygen. These authors showed that even with the crude ionic potential the basic structure of silica glass as a random network of corner connected silica tetrahedral is achieved in the MD simulation. The WCA potential was re-parameterized and the charges reduced by one of authors[9] and Mitra et al. used the Pauling form for the two-body potential[10]. Later three-body terms were added and parameterized to reduce the spread in the OSiO bond angles and more importantly to adjust the tetrahedral corner sharing SiOSi bond angles so that these angles agree even more closely with the experimental values deduced from the neutron scattering peaks[11 12 13]. The more recent group of force fields including BKS have been based on fits to quantum mechanical calculations. Carre et al.[14] re-parameterized the BKS potential (hereafter referred to as the CHIK potential) to fit the structures they obtained using density functional Car-Parrinello MD simulations. Still other potentials based on *ab-initio* calculations have been

[5] R. Bruckner, J. Non-crys. Solids **5**, 123-175 (1970).
[6] K. Vollmayr, W. Kob and K. Binder, Phys. Rev. B **54** 15808-15827 (1996).
[7] C. A. Angell, Science 267, 1924 (1995); K. Ito, C. T. Moynihan and C. A. Angell, Nature 398, 492 (1999).
[8] L. V. Woodcock, C. A. Angell and P. J. Cheeseman, J. Chem. Phys., 65, 1565-1577 (1976).
[9] T. F. Soules, J. Non-crys. Solids 123, 48-70 (1990).
[10] S. K. Mitra, M. Amini, D. Fincham and R. W. Hockney, Phil. Mag. B, 48, 365-372 (1981).
[11] B. P. Feuston and S. H. Garofalini, J. Chem. Phys. 89, 5818-5824 (1988).
[12] P. Vashishta, R. K. Kalia and J. P. Rino, Phys. Rev. B 41, 12197-12209 (1990).
[13] A. A. Hassanali, S. J. Singer, J. Phys. Chem. B, 111, 11181-11193 (2007).
[14] A. Carre, J. Horbach, S. Ispas and W. Kobb, EPL, 82, 17001 (2008).

proposed[15] [16] including potentials that require the force field to be modified at each time step in the MD run[17]. The Tagney and Scandolo (TS) [17] potential that evaluates the polarizability of ions at each time step based on the neighboring ion configuration has been shown to give very good agreement with infrared spectra. Paramore et al. [18] attempted to map the TS force fields onto a new pairwise potential. These potentials have been compared[19]. Demicralp, et al. used a combination of a Morse potential and Coulombic interactions and allowed the Coulomb charges to vary based on a valence-averaged and electron affinity equation during the run[20]. A potential almost identical to that used by Demicalb was used later by Takada, et al.[21] with fixed charges to simulate silica glass. Although non-linear effects requiring the force field to be updated at each time step must be important in the limit, for example, of vaporization of SiO_2 into SiO and O_2 molecules, in keeping the limited aim of this article to find simple practical potentials for large scale MD simulations of silica we focus on only simple pairwise force fields that are not adjusted during the MD run. Our objective is limited to finding a practical and efficient perhaps empirical set of pair force field that is able to predict a specific set of properties over the temperature range and heating of the laser mitigation experiments.

This paper is organized as follows: After briefly describing the methods used, we graph four different simple two-body pair force fields chosen both for their simplicity and efficiency in MD runs and for covering a wide range of Si-O bond strengths. Then the results of NPT MD runs heating and cooling the canonical ensembles with each of the potentials are presented. We estimate the thermodynamic melting temperature for simulated β-crystobalite ensembles by equilibrating the liquid and solid in a separate set of simulations. Fictive temperatures during cooling are determined from the break in the slope of the enthalpy curves and the glass transition and heat capacity behavior is discussed in the final

[15] S. Tsuneyuki, M Tsukada, H. Aoki and Y. Matsui, Phys. Rev. Lett., 61, 869 (1988).
[16] M. Benoit, S. Ispas, P. Jund and R. Jullien, Eur. Phys. J. B 13, 631-636 (2000).
[17] P. Tangney and S. J. Scanolo, J. Chem. Phys. 117, 8898-8904 (2002).
[18] S. Paramore, L. Cheng and B. J. Berne, J. Chem. Theory Comput. 4, 1698-1708 (2008).
[19] D. Herzbach, K. Binder and M. H. Muser, J. Chem. Phys 123, 124711 (2005).
[20] E. Demiralp, T. Cagin and W. A. Goddard III, Phys. Rev. Letters, 82, 1708 (1999).
[21] A. Takada, P. Richet, C. R. A. Catlow and G. D. Price J. Non-crys. Solids, 345-346, 224-229 (2004).

section. The density versus temperature and self diffusion coefficients are also presented for each force field. The conclusion of this study is that the potentials so far designed to fit *ab-initio* calculations, such as, BKS give melting and glass forming temperatures that are too high. A simple softer pairwise potential can fit the experimental melting and cooling results for silica glass and liquid quite well. However, all the potentials except those with extremely high melting temperatures and fictive temperatures give activation energies for self-diffusion that are too low by comparison with the activation energy for viscosity.

II METHOD

A. MD Methods

All the MD simulations reported here were carried out using LAMMPS, a MD software code for parallel processing computers developed at Scandia National Laboratory[22]. All runs were made under NPH conditions[23] with pressure maintained at ~1 atmosphere and with heat added or subtracted using the Langevin method[24] with weak coupling to random thermal bath simulating an NPT canonical ensemble. In most of the simulations, we started with MD ensembles of 1000 Si atoms and 2000 O atoms initially at their positions in an idealized β-cristobalite configuration and used the Verlet algorithm with a time step of 1 femtosecond for the MD runs.

Arguably the most difficult problem in setting up these MD simulations is how to treat the long-range Coulomb forces. LAMMPS has two built in options for long range Coulomb forces: a solution of the Ewald equation and a particle-particle particle mesh (PPPM) solver where the mesh is generated from a numerical solution of Poisson's equation. However, both are computationally intensive and difficult to apply to surfaces. After doing many of our calculations with both options, we adopted a screened potential proposed by one of the authors[9] wherein the Coulomb force is replaced by the force field of a

[22] S. J. Plimpton, J. Comp. Phys. 117, 1-19 (1995).
[23] H.C. Anderson, J. Chem. Phys. 72, 2384 (1980).
[24] T. Schneider and E. Stoll, Phys Rev B, 17, 1302 (1978).

charge at the center of a sphere containing uniform charge density of opposite sign. The uniform charge density spheres will cancel in a random system[9]. This can be checked by increasing the radius of the sphere. Carre, et al.[25] recently compared two other methods for screening the long range part of the BKS potential, the Wolf summation and Yakawara equation, and showed that with a screening distance of 10.58 Å the dynamics and structure were essentially the same as that obtained using the full Ewald potential. Using our simple screening, we obtained the same structures and dynamical properties as with the Ewald and PPPM solutions in LAMMPS when using a cutoff of 11.0 Å. Even with this rather long range cutoff these calculations ran ~ 20 times faster than those using the Coulomb solvers included in LAMMPS, and with the cutoff used earlier[9] of 5.5 Å the calculations ran another factor of 20 times faster.

B. Force Fields

The equations for the force fields investigated are shown in Table 1. They include three previously published force fields[3 14 21] and an empirical pairwise force field used by one of the authors[9]. The empirical potential can be scaled without significantly disturbing the calculated structure. We report results using a scaling factor of 0.65 in order to investigate a second soft field. The BKS and CHIK equations include a $1/r^7$ term that must have another term added to prevent the force from diverging at small values of r[6 14].

[25] A. Carre, L. Berthier, J. Horbach, S. Ispas and W. Kob, J. of Chem. Phys. 127 114512 (2007).

$$F_r = AB\exp(-Br) - 6C/r^7 + (q_i q_j e^2/r^2)(-r^3/r_{cutoff}^3) \quad (1)$$

	q_{Si}	r_{cutoff}	Si-O			O-O			Si-Si		
			A(eV)	B(Å^{-1})	C(Å^6)	A(eV)	B(Å^{-1})	C(Å^6)	A(eV)	B(Å^{-1})	C(Å^6)
BKS	2.4	11.0	18004	4.473	133.5	1388.	2.76	175	0	0	0
CHIK	1.910	11.0	27029	5.158	148.1	659.6	2.590	26.84	3150.1	2.852	626.8
Soules*	2.28	5.5	608.55	3.448	0	466.6	3.448	0	0	0	0

$$F_r = -2AB[-\exp(B(C-r)) + \exp(B(C-r))] + (q_i q_j e^2/r^2)(-r^3/r_{cutoff}^3) \quad (2)$$

	q_{Si}	r_{cutoff}	A(eV)	B(Å^{-1})	C(Å)	A(eV)	B(Å^{-1})	C(Å)	A(eV)	B(Å^{-1})	C(Å)
Takada	1.3	11.0	1.996	2.652	1.628	0.0233	1.373	3.791	0.0077	2.045	3.760

Table 1 Equations and parameters for the force fields compared in this work. Soules* is from ref. 9, Eq. 9 page 51[9] converted to present units and scaled by 0.65 with the Si-Si short range repulsion set equal to 0.

The pairwise force field equations are graphed in Figure 1. The maximum attractive SiO force fields span a wide range from what might be called the two strong attractive Si-O force fields (BKS and CHIK) to two soft force fields (Takada and the scaled Soules' empirical force field). This is also reflected in the integral, the pair-wise potential energy curves. The graphs also show differences in the curvature of the Si-O force field going from broad to narrow depending on whether an additional attractive term was added to the Coulomb. On the figure are activation energies which are defined as the potential energy differences between the pairwise SiO potential energy evaluated at the equilibrium distance in the simulations, ~1.62 Å, and the potential energy at the inflection point or the maximum restoring force. When a SiO bond is stretched to beyond this distance the SiOSi potential bifurcates and

the oxygen atom midway between two silicon atoms will accelerate toward one or the other. We view this energy as a measure of the bond breaking activation energy and it will be seen to roughly track properties, such as, the activation energy for diffusion discussed later.

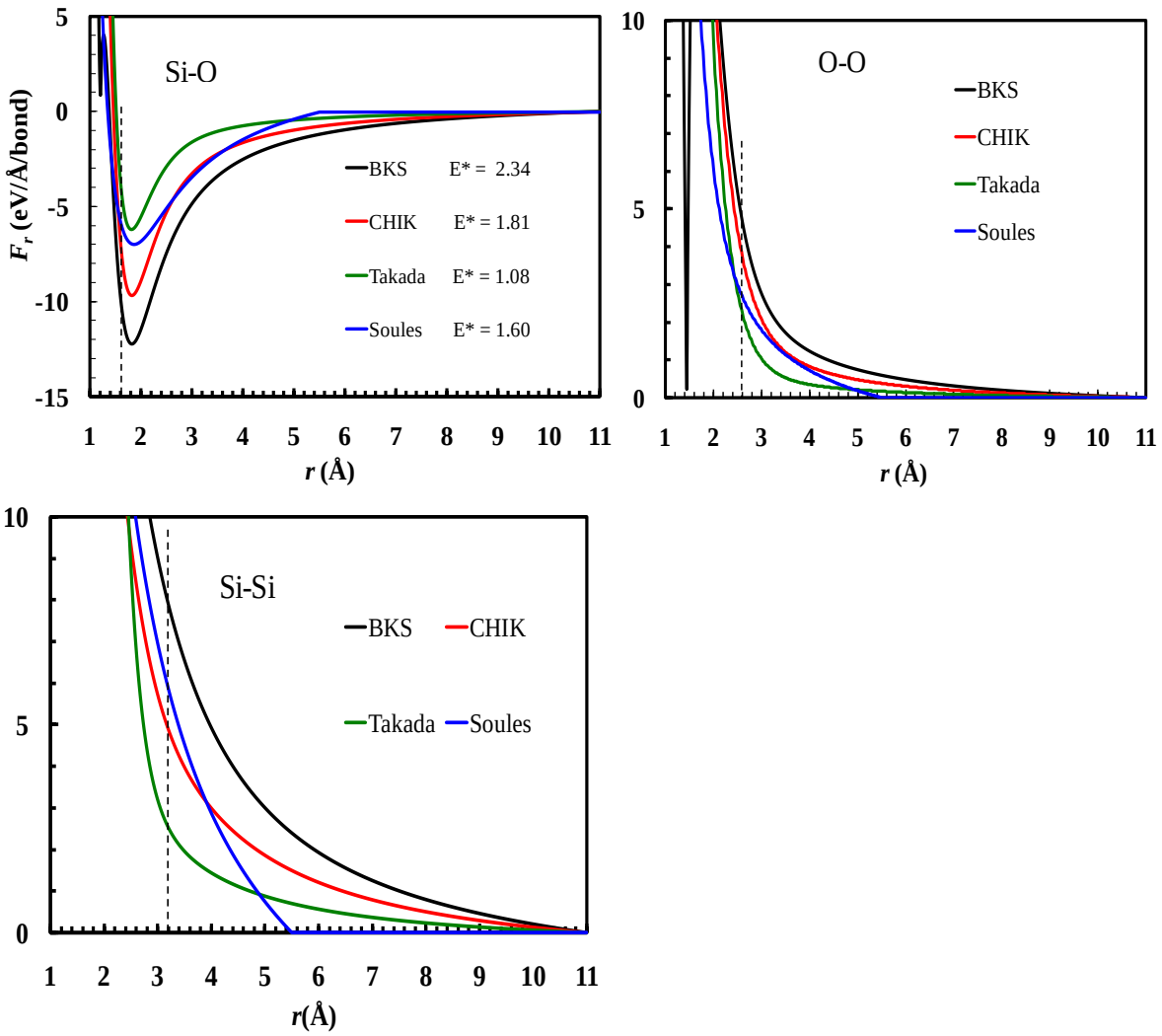

Figure 1 Graphs of the radial force fields being compared. The dashed lines indicate values at the nearest neighbor distances. The numbers labeled E* are activation energies in eV/atom determined as difference in potential energies between the equilibrium positions and the point of inflection in the potential energy curves.

The O-O force field generally has an additional repulsive term added to the Coulomb repulsion keeping the oxygen atoms well separated and maintaining the OSiO bond angle at the tetrahedral value,

109^{o}. From the graphs it is not clear why several of the authors have also included an attractive OO force field term since this is overwhelmed by the repulsion.

The Si-Si force field is repulsive and in the BKS and modified Soules potential it is assumed to be entirely due to the Coulomb repulsion between the charges. Deleting additional attractive and repulsive terms to the Si-Si force from other force fields has little effect on Si-Si force field especially at distances near the closest Si-Si distance, ~ 3.15 Å.

III. RESULTS

A. Melting

Figure 2 compares the enthalpy versus temperature curves for each of the four force fields during heating of the MD canonical ensembles starting with the idealized β-crytobalite structure for 3000atoms.. The heating rates are ~ 4000 ^{o}K/ns. The small steps or kinks in the curves indicate a small heat of fusion in the enthalpy curves at the homogenous melting temperature. The insert shows that, not surprisingly the temperature at which homogenous melting occurs depends on the heating rate.

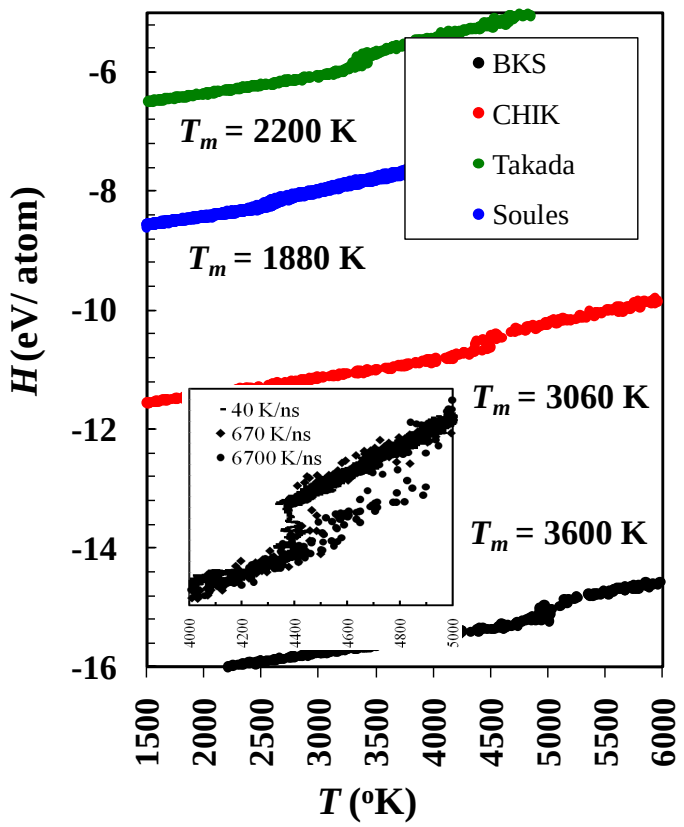

Figure 2 Enthalpy versus temperature during heating of the MD ensembles for the four force fields. Kinks in the curves indicate the homogenous melting temperatures when the MD heating is carried out at 4000°K/ns. Insert shows effect of heating rate on the melting temperature with BKS potential. T_m is estimated thermodynamic melting temperatures of the MD ensembles using the methods discussed in the text.

Because MD heating rates are always much faster than experimental heating rates (except perhaps in some of our laser heating experiments) and because there are no nucleation sites in the MD simulation thermodynamic melting temperatures were estimated using a different approach. An equilibrium between the crystal and liquid was established without introducing a surface area driving force or a critical size seed by splitting the MD ensemble representing β-cristobalite in half with the atoms in the top half of the atoms labeled "crystal" and those in bottom labeled "glass". The glass layer atoms are heated to above the homogenous melting temperature while the crystal layer atoms were kept at a low temperature using the Langevin coupling. Because of the periodic boundary conditions in the MD simulations this simulated a layered structure. While this cannot be done in the laboratory it is easy to

achieve in the MD simulation. NPT conditions were used with the pressure set at 1 atmosphere in each direction.

In one set of MD experiments the Langevin terms were then turned off allowing the temperature of the glass and crystal atoms to equilibrate. Depending on the choice of initial temperatures for both layers it was possible to get the crystalline ensemble to partially melt so that the crystalline and amorphous phases were in equilibrium. The equilibrium temperature was independent of the initial temperatures chosen so long as the system did not completely melt. A cross section of the configuration of such an ensemble before and after being allowed to equilibrate is shown in Figure 3. The difficulty in these experiments was being able to run long enough to make sure the entire system did not melt. Runs up to 10 nanoseconds (10 million time steps) were used.

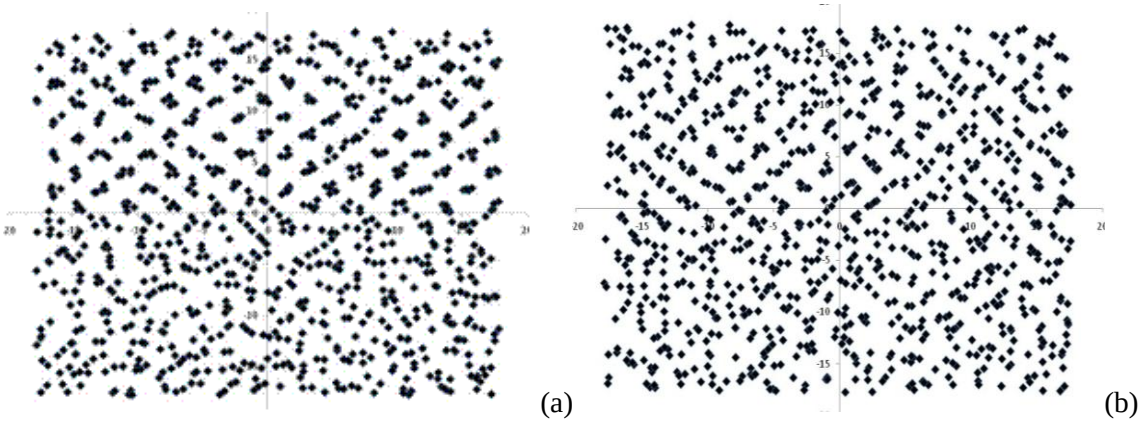

Figure 3 Cross section through a silica MD ensemble in which the atoms of the upper half are held at a temperature below the spontaneous melting temperature and the lower half is heated above the melting temperature. Figure 3 (b) shows a snapshot after allowing the two layers come to an equilibrium temperature. The liquid crystal interface has moved into the crystal region indicating some melting of the crystal. Because the oxygen atoms show more disorder only the silicon atoms are shown.

A clearer estimate of the melting temperature is achieved by taking the ensemble after melting every other layer rescaling the velocities of all the atoms to a suitable temperature below the melting point and then raising the temperature of the entire ensemble of glass and crystal atoms slowly using velocity rescaling. This procedure is the same as was done for homogenous melting but the crystal layers are in direct thermal contact with an amorphous phase. Melting was still sometimes difficult to observe in our

usual 3000 atom cubic box during the heating. The influence of the large area to volume ratio of glass surface layers appeared to induce melting at lower temperatures even though there should have been no surface area driving force. Whether melting temperatures can be influenced by having very thin (< 20 Å) alternate layers of glass/liquid and solid is not known. The phenomena observed may be closer to a reverse sintering than thermodynamic melting.

A stable melting point independent of the simulation time was achieved by increasing the simulation cell thickness decreasing the fraction of surface atoms by a factor of 2 and 4 by constructing taller rectangular prisms for the simulation cells. Taller prisms cells with a distance between layers of glass and crystal in contact of 35.8 and 71.6 Å containing 720 and1440 silicon atoms respectively with the corresponding number of oxygen atoms were used. Figure 4 shows an example using the CHIK force fields. In order to increase the temperature as slow as possible in these runs the force fields were modified by setting the long range cutoff for the Coulomb potential at 5.5 Å. The heating rate was 10-100 ^{o}K/ns.

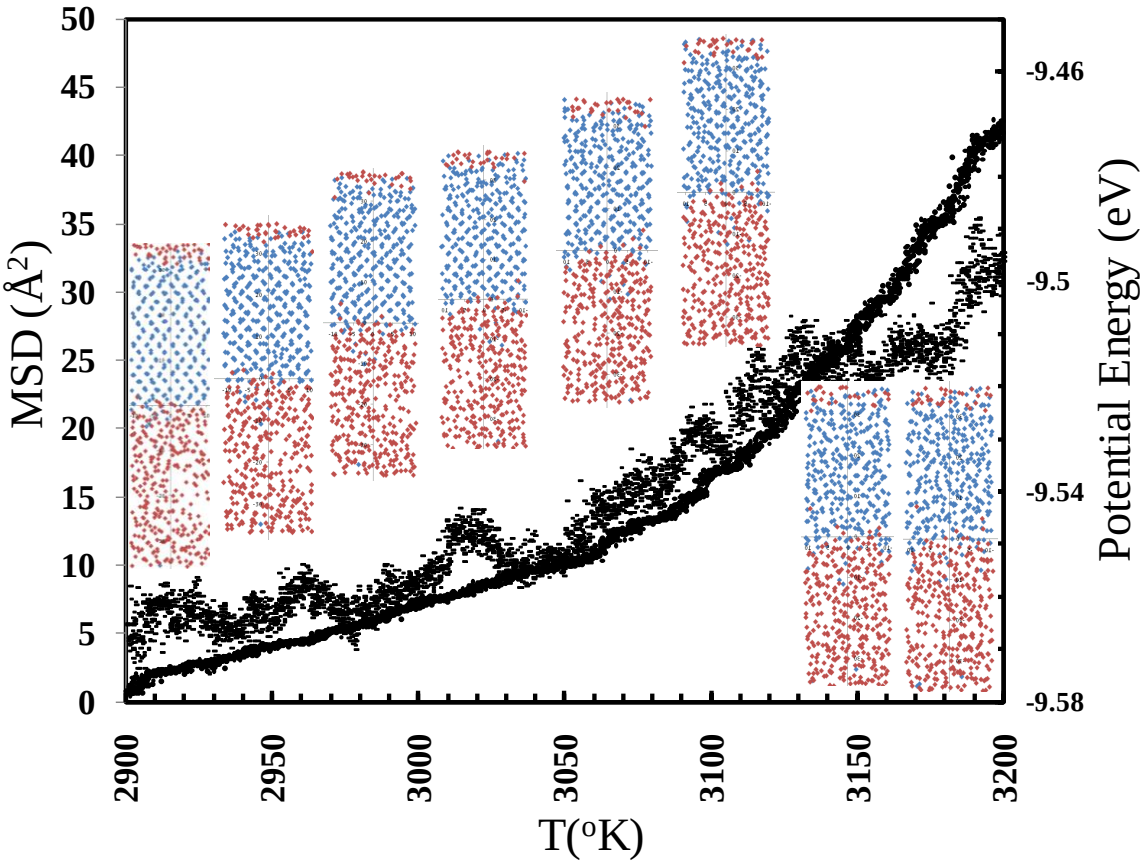

Figure 4 Simulated MD melting of an ensemble of β-crystobalite (showing Si atoms as blue diamonds) in contact with a melted SiO_2 glass (red diamonds) at the same temperature using the CHIK force field and a heating rate of 300 °K/ns. The potential energy versus temperature of the system is the data with scatter. The smooth curve is the mean squared displacement (MSD) of the crystal atoms versus temperature. Melting is determined by the break in the MSD curve, movement of front of disorder in the lattice and a change in slope of the potential energy.

Melting is observed where the MD β-crystobalite atoms near the interface start to become amorphous and the surface between the crystal and the amorphous regions starts to move. The CHIK β-crystobalite ensemble is starting to melt while in equilibrium with the amorphous phase between 3000 and 3100 K. Another indicator of melting is a change in slope of the potential energy curve for all the atoms. Below the melting temperature, the increase in potential energy of the crystal is with temperature is small. Just before melting begins the potential energy curve of the whole system becomes noisy and then the slope increases as more atoms go into the amorphous phase. Also the mean squared

displacement of atoms in the crystal group after an initial increase due to vibration and a subsequent increase due to increasing diffusion in the crystalline solid begins to increase dramatically when the melting starts and ultimately catches up to the displacement of atoms in the glass/liquid. The theoretical curve for diffusion in the glass during a linear ramp when displaced to the melting temperature is a reasonable fit to the long time slope of this mean squared displacement curve. These simulations were used to determine the melting temperatures for the different potentials indicated on Figure 2.

The melting temperature determined in this way for BKS β-cristobalite at 1 atmosphere is 3600 K in good agreement with Saika-Voivod, et al.[4] who determined the melting points of BKS quartz and coesite at one atmosphere by calculating where the free energy of the crystal and glass are equal while the experimental melting temperature of β-cristobalite is 1978 K. The MD melting point determined as described above for the Takada force field is only ~ 10 % higher than experiment and the melting point for the scaled Soules potential is actually less than the experimental melting point.

B. Cooling and Fictive Temperatures

Figure 4 shows the enthalpy versus temperature curves during cooling at a rate of 1000 ^{o}K/ns The fictive temperatures indicated on the figure are the temperatures at which a linear extrapolation of the solid properties, in this case the enthalpy intersects an extrapolation of the liquid curve. In experiments and in simulations the fictive temperatures decrease with a decrease in the cooling rate. The shift to lower temperatures of the fictive temperature with decreasing MD cooling rates in silica simulations was first shown by Soules[9] for a simple empirical potential and discussed in detail by Vollmayr, et al.[6] for the case of the BKS silica potential and so will not be presented here.

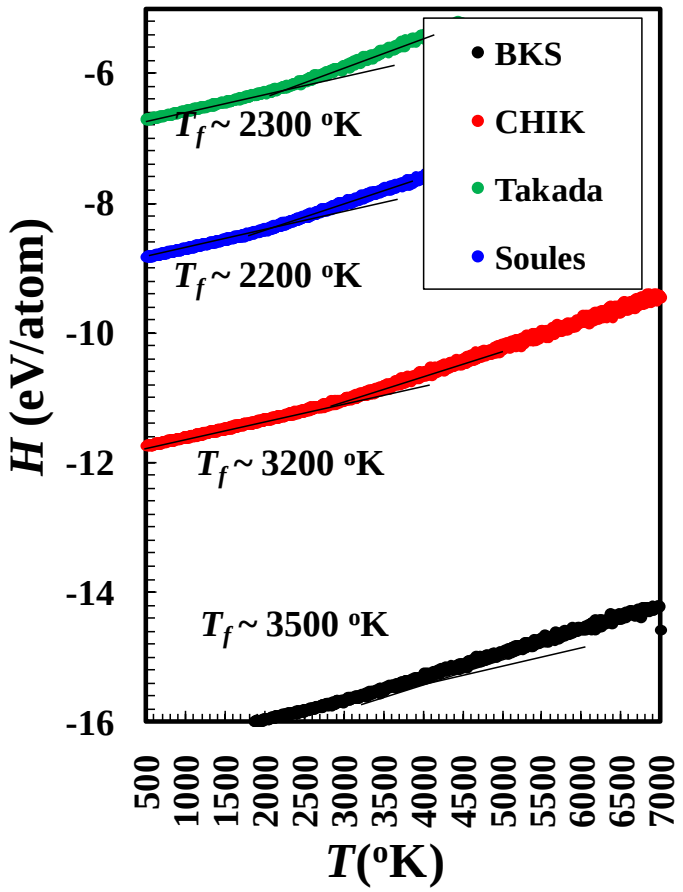

Figure 5 Enthalpy versus temperature during cooling of MD silica glass runs under NPH conditions at 1000 °K/ns. T_f , the fictive temperatures, are the temperatures at which the liquid configuration is arrested on the time scale of the cooling indicated by the intersection of extrapolations of the solid and liquid curves.

Because of statistical noise in the enthalpy data heat capacity curves shown in Figure 6 were obtained by first fitting the low temperature data to a line. The difference between the enthalpy data and the line at higher temperatures was fit to a low order polynomial and the sum was differentiated to give the curves.

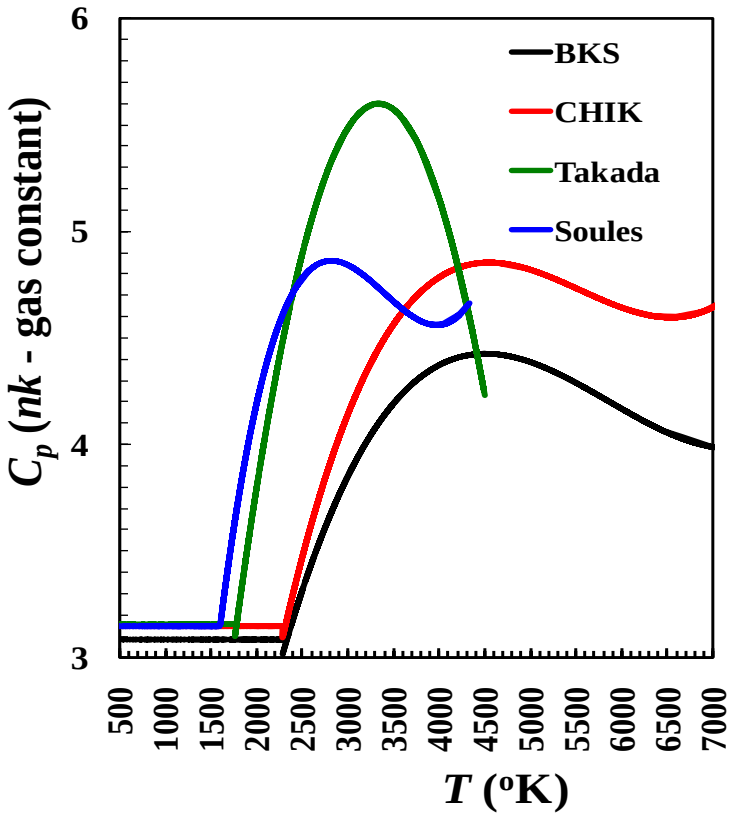

Figure 6. Heat capacity, C_p, curves obtained by taking the derivative of the enthalpy curves in Figure 4 as discussed in the text.

C. Density

A very interesting property of silica and some other random tetrahedral network glasses that should be reproduced in a practical MD model is the small thermal expansion of silica glass over much of its solid glass temperature range and the density maximum in the liquid[26]. Both phenomena are easily understood qualitatively from a sketch (see Figure 7) illustrating corner sharing randomly connected silica tetrahedra that form rings with predominantly six tetrahedra per ring. The rings are the ribs of an open fused cage-like structure. Vibrations of the oxygen atoms perpendicular to the Si-O-Si bonds connecting tetrahedral are readily thermally excited and will rock the tetrahedral making up the cage ribs but will not increase

[26] R. Bruckner, J. Non-Cryst. Solids 5, 123-175 (1970).

the volume. When the vibrations are strong enough or when tetrahedra actually break away from ribs in the liquid, the specific volume will collapse slightly to higher density amorphous structures.

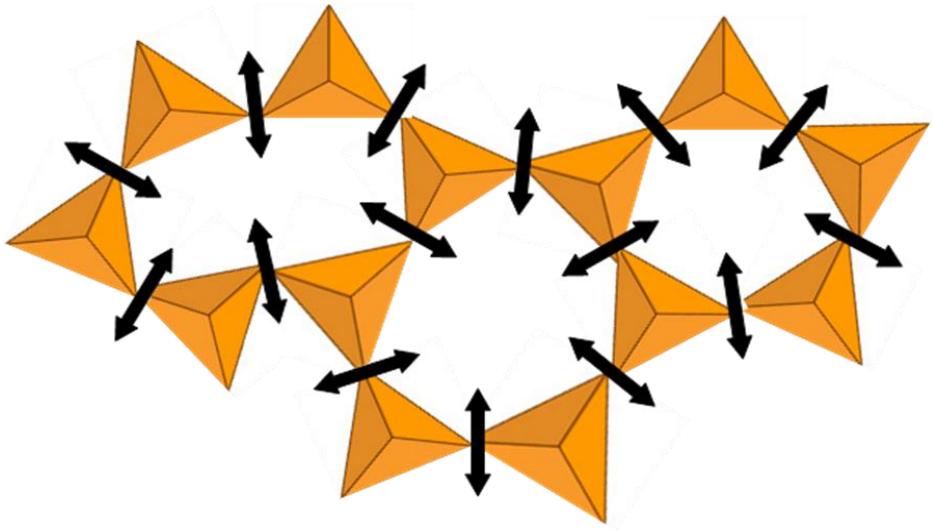

Figure 7 Sketch illustrating the ring structure of vitreous silica with corner connected tetrahedral. The figure shows the low energy rocking modes of oxygen atoms perpendicular to the axis between silicon atoms.

Figure 8 shows how the density varies as MD runs are cooled using each of the force fields investigated. The experimental density at room temperature is 2.2 g/cm^3.

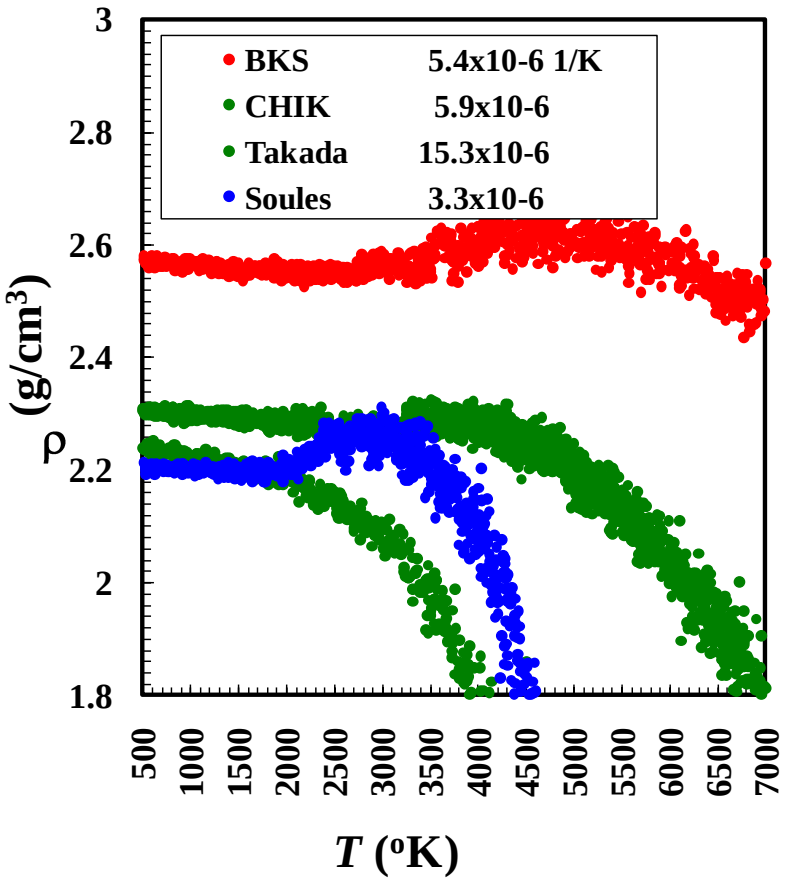

Figure 8 Density during MD cooling for each of the force fields tested. The numbers in the legend are volumetric thermal contraction coefficients per degree K in the solid temperature range (300-1500 ^{o}K).

All force fields except the BKS give very close to the experimental density at room temperature. Vollmayr, et al truncated and shifted the short range terms in the BKS potential to correct the room temperature density[6]. Also while all the force fields result in a small thermal expansion in the solid glass temperature range the volume thermal expansion coefficients are still significantly larger than the experimental value ~ 1.6×10^{-6} $^{o}K^{-1}$. Takada et al. argue that their potential also gives a very small 0.1 % increase in density near 1700 ^{o}K [21] but the thermal expansion of this force field is relatively large and the density maximum was not convincing in our simulations. On the other hand the other force fields show a distinctive increase in density, greater than has been observed experimentally. We believe that this increase requires an attraction between the silicon atoms and the next nearest neighbor oxygen atoms

encouraging the structure to collapse when vibrations disrupt the corner sharing tetrahedral rings. This next nearest neighbor distance as shown below is ~ 4.0 Å. The Takada force field shows very little Si-O attraction at this distance while the other force fields investigated probably have too strong a longer range Si-O attraction at ~ 4 Å.

D. Pair radial distribution functions (rdf's)

There are many similarities between the structures calculated from all these force fields in spite of the very different strengths of the pairwise potentials. All of them give the same overall structure for vitreous silica, namely, silica tetrahedral with a Si-O distance of ~1.61 Å linked at corners and in rings of predominately 6 members forming the ribs of an overall fused cage-like structure. This shows that these features are mainly a function of relative atomic sizes.

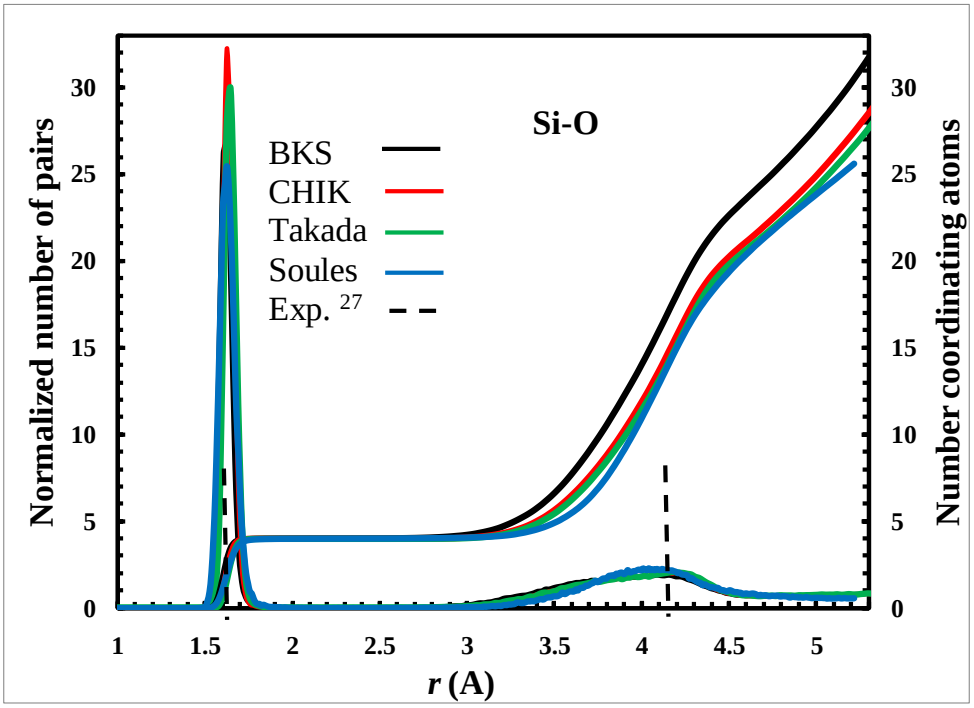

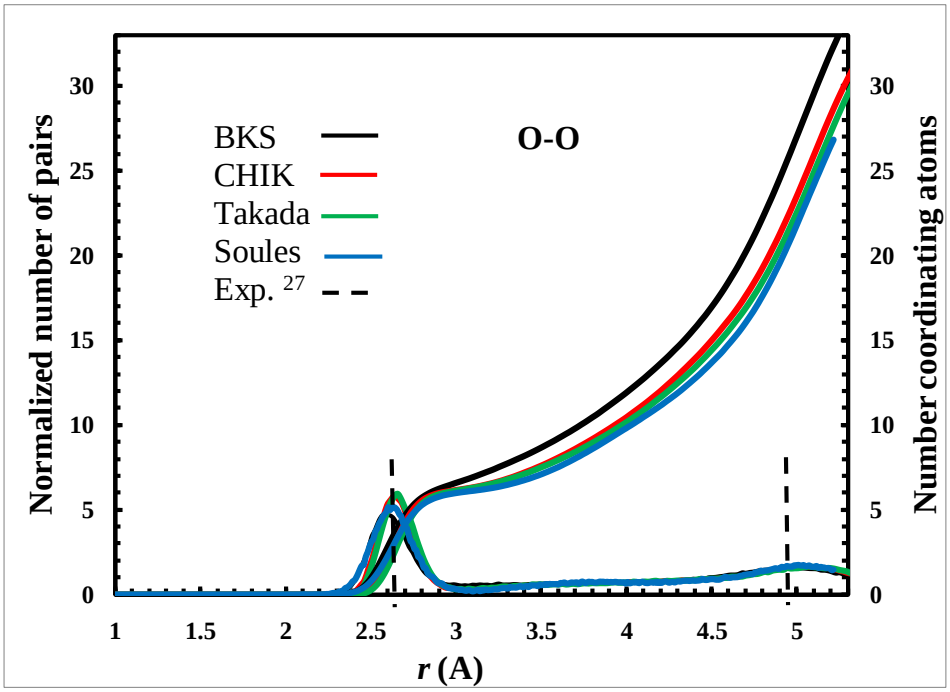

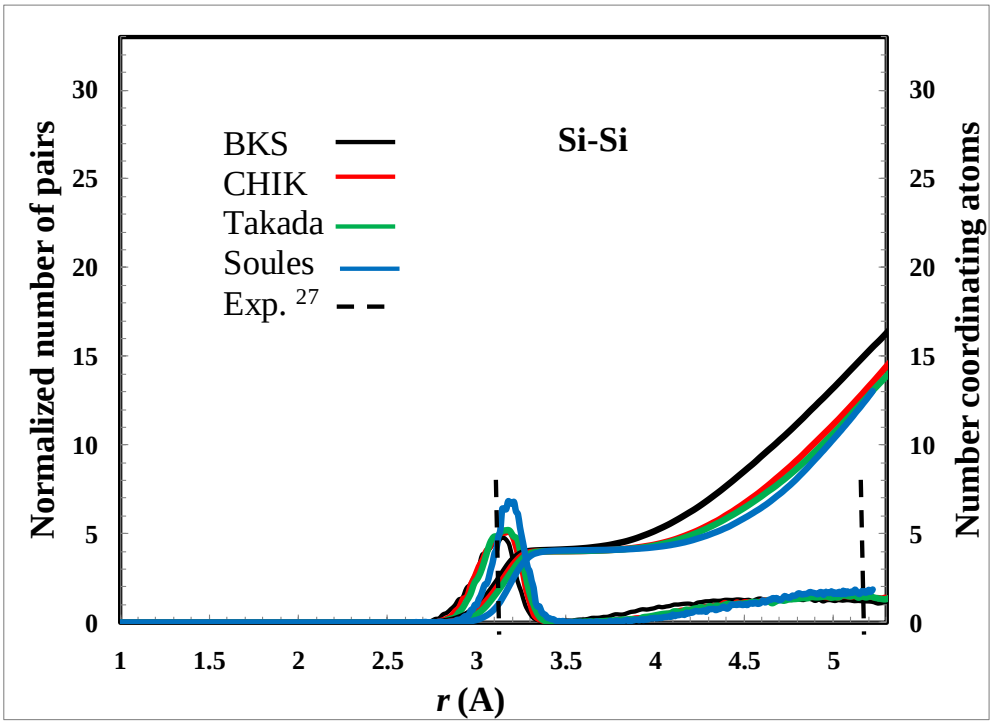

Figure 9 The pair radial distribution functions at room temperature from MD cooling simulations. Also shown are the cumulative number of neighboring atoms as a function of distance.

There are some significant differences. For example the first Si-O peak in our empirical potential is significantly broader than either experiment or the first peak of the other models. The BKS model shows higher coordination numbers at next nearest neighbor distances which is consistent with the higher density obtained with this potential. More detailed structural analyses of the MD rdf's are given by the respective authors. Suffice it to say that if you a modeler you are amazed at how close the calculated rdf's are to the x-ray diffraction[27] and the neutron diffraction correlation functions[28] even though in the case of the more empirical potentials the parameters were chosen to insure that at least the most probable nearest neighbor Si-O and O-O distances are correct. On the other hand the experimentalist is often noticing differences[29] for example in bond angles, such as the Si-O-Si bond angle that is deduced from experiment to be peak around 140 degrees while most of the simulations give a value of ~ 150 degrees. Certainly effects, such as, repulsion by non-bonding electron pairs on the bridging oxygen atoms that would reduce this angle are real and are not included in these simple radial pairwise force fields. They can be included in three-body potentials but at the expense of adding additional adjustable parameters or mapping out a force field in a many dimensional space.

E. Self-diffusion coefficients

Diffusion constants are easy to obtain from atomic mean squared displacements in MD simulations. The mean square displacement of atoms from some initial position quickly rises and plateaus displaying vibration motion and then continues to rise linearly and the slope of this long time graph measures the diffusion constant, $D_i \Rightarrow (1/6)d\left\langle(\vec{x}_i(t)-\vec{x}_i(0))^2\right\rangle/dt$. Figure 8(b) shows that for all the potentials investigated the self-diffusion of silicon atoms tracks the self-diffusion of the oxygen atoms although in the case of our empirical potential for which the Si-O bonding is much broader the oxygen

[27] R. L. Mozzi and B. E. Warren, J. Appl. Cryst. 2, 164 (1969).
[28] D. I. Grimley, A. C. Wright and R. N. Sinclair, J. Non-Cryst. Solids 119, 49 (1990).
[29] A. C. Wright, J. Non-Crys. Solids 159, 264-268 (1993).

atoms diffuse about twice as fast as the silicon atoms. The self diffusion coefficients fall in two groups one corresponding to the "strong" potentials and the others the weak potentials. Activation energies are roughly twice the activation energy estimates from Si-O potentials in Figure 1 suggesting that self diffusion of either Si or O atoms requires the breaking of two bonds.

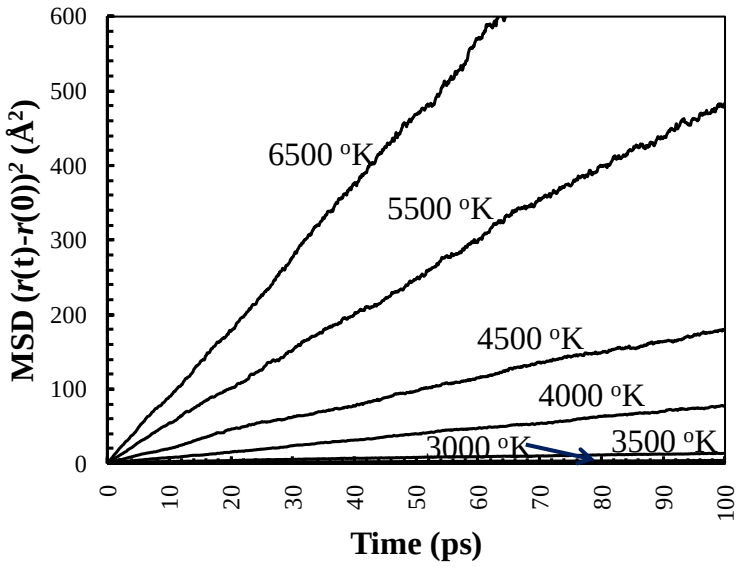

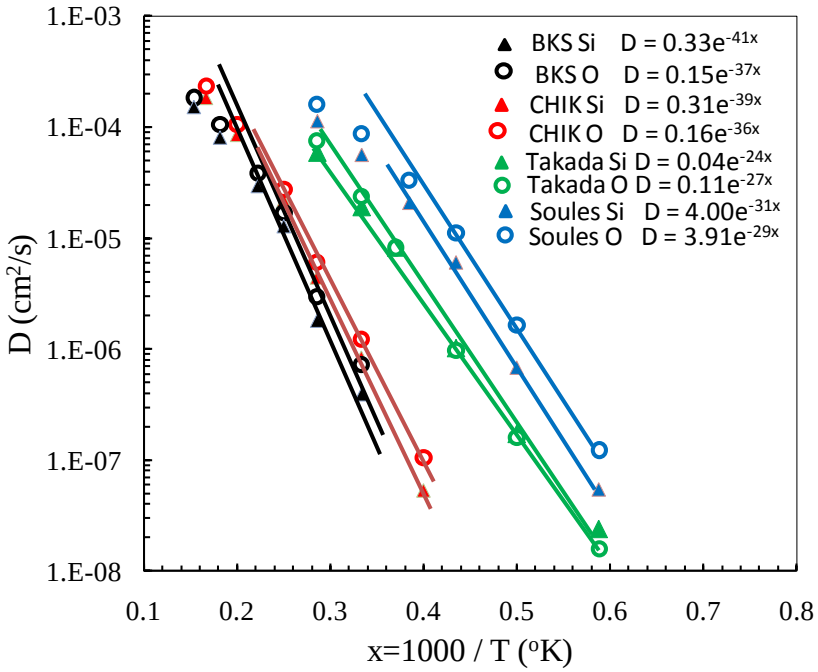

Figure 10 The figure on the left is a sample of the mean square displacements of atoms at different temperatures, in this case Si atoms using the BKS potential. The MD ensemble was cooled to each temperature indicated in the curves and then run for 100 psec. The graphs on the right are diffusion constants obtained from the long time slopes of the mean square displacements.

The diffusion coefficients for the BKS potential shown in Figure 8(b) are in agreement with those determined by Shell, et al.[30] and Saika-Voivod et al.[31] . Also like the results of Saiko-Voivod, et al. our diffusion results for all the potentials when plotted as lg (D) versus 1/T show a curvature at high temperatures, $D < 10^{-5}$, becoming Arrhenius at lower temperatures, $D > 10^{-6}$. Saiko-Voivod et al. account for this curvature in the case of the BKS force fields by using the Adam-Gibbs expression for the relaxation, $D/T = \mu_0 \exp(-A/TS_C)$. They plotted $\lg(D/T)\ \text{versus}\ 1/TS_C$ using S_C evaluated from their MD data (see Eq. 6 below).

Finally Bulk moduli for each force field was determined by compressing the MD simulated silica glasses at 293 K. Only small reductions in volume were made to avoid any coordination change. All force fields except the soft potential from Takada[21] give Bulk moduli that are too high by ~ 30-40%.

Model	Bulk modulus (GPa)
BKS	58.7
CHIK	54.3
Takada	43.5
Soules	55.8
Experiment	~39

Table 2. Bulk moduli, $B = (1/V)(\partial V/\partial T)$, obtained by reducing slightly in steps the volume of the MD simulation box at room temperature.

IV. DISCUSSION

[30] M. S. Shell, P. G. Debenedetti and A. Z. Panagiopoulos, Phys. Rev. E 66, 011202 (2002).
[31] I. Saiko-Voivod, F. Sciortino, T. Grande and P. H. Poole, Phil. Trans. R. A , 363, 525-535 (2005).

A. Fictive Temperatures

The high fictive temperatures shown in Figure 5 are not surprising. Using the phenomenological non-linear Tool-Narayanaswamy[32] equations to calculate the fictive temperature with reasonable values for the parameters (actually we used values selected by the authors rather than those of Brunning, et al.[33] that were obtained by fitting actual relaxation data but at much slower cooling rates), one predicts fictive temperatures of >2600 K at a cooling rate of 1000 ^{o}K/ns[34]. The equation for the fictive temperature is given by:

$$
\begin{aligned}
&T_f = T - \int_{T_o}^{T} M(T', T_f, t)\, dT'; \\
&M = \exp[-(t/\tau)^{\beta}]; \\
&\tau \sim \tau_{ref} \exp\left[H/R \left(1/T_{ref} + x/T + (1-x)/T_f \right) \right] \qquad H/R \sim 73kK; \qquad x \sim 0.7; \qquad \beta \sim 1.0. \\
&\mathrm{P}(T_0) - \mathrm{P}(T) = \alpha_s (T_0 - T) + (\alpha_l - \alpha_s)(T_0 - T_f).
\end{aligned}
\tag{3}
$$

Where τ_{ref} is the structural relaxation time measured at a reference temperature T_{ref}. Relaxation curves have been measured by monitoring the D_2 Raman peak intensity in a furnace[35]. x is a parameter that weights the fictive temperature effect on the activation energy and β is the Kohlrausch-Williams-Watts stretched exponential decay parameter. P(T) is the value of a property that depends on the structural properties of the glass. The last equation assumes that the derivatives of the property in the liquid l and solid state s are constant over the temperature range of interest. If they are not then this latter equation must be replaced by an integral over the temperature range.

However, Vollmayr, et al.[6] convincingly show that these equations must be at least modified to describe the very high temperatures and the very rapid cooling rates of MD simulations. Following

[32] O. S. Narayanaswamy, J. Amer. Ceram. Soc., 54 491-498 (1971).
[33] R. Bruning, C. Levelut, A. Faivre, R. LeParc, J. –P Simon, F. Bley and J. –L Hazelmann, Europhys. Lettt., 70, 211-217 (2005); R. Brunning, C. Levelut, R. Le Parc, A. Faivre, L. Semple, M. Vallee, J. –P Simon, J. –L. Hazeman, J. Appl. Physics, 102, 083535 (2007).
[34] For an algorithm to solve Eqs. 3, see A. Markovsky and T. F. Soules, J. Amer. Ceram. Soc., 67, C-56-57 (1984).
[35] D. D. Goller, R. T. Phillips and I. G. Sayce, J. Non-crys. Solids 355, 1747-1754 (2009).

Stillinger and Weber[36], steepest descent quenching of MD runs show the properties of the inherent mechanically stable structures of the potential energy landscape without kinetic energy effects. The densities of the inherent structures selected at different temperatures vary when the temperature from which the quench is made is between 4840 ^{o}K and 3200 ^{o}K. However, the densities of inherent structures quenched from temperatures > 4840 ^{o}K are the same as if they had been quenched from 4840 ^{o}K. It was not possible to fall out of equilibrium with the liquid and into a different mechanically stable solid structure corresponding to temperatures greater than 4840 ^{o}K due to the limited range of mechanically stable energy minima. This would be equivalent to in the phenomenological Eqs. (3), above 4840 ^{o}K, always making the relaxation function instantaneous or in another interpretation assuming that at temperatures above 4840 ^{o}K the derivative of the property in the equilibrium liquid loses its configuration contributions. The latter interpretation is supported by the shape of the heat capacity curves shown in Figure 6. Configuration contributions to the heat capacity decline past the peak in heat capacity curve. Configuration contributions to the heat capacity can be frozen in only from temperatures near the peak in the heat capacity curve down to lower temperatures. However this fictive temperature range is dependent on the choice of the potential. Useful potentials should be chosen so that different inherent structures are selected in the range of say ~1300 – 2300 ^{o}K , a range over which changes in density[37] and other fictive temperature dependent properties, such as, the Raman bands have been measured[38].

B. Statistical Mechanical Model of Liquid MD Silica

The equilibrium liquid/glass graphs of energy and heat capacity (Figures 5 and 6) can be understood assuming that the liquid samples a 3N dimensional potential energy hyper-surface where N is

[36] F. H. Stillinger and T. A. Weber, Phys. Rev. A 25, 978 (1982); Science 225, 983 (1984); F. H. Stillinger, Science 267, 1935 (1995).
[37] J. E. Shelby, J. Non-crys. Solids 349, 331-3336 (2004).
[38] A, E. Geissberger and F. L. Galeener, Phys. Rev. B, 28, 3266-3271 (1983).

the number of atoms with many minima corresponding to mechanically stable amorphous structures[36]. In the classical limit,

$$H(T) = E_{harm}(T) + E_{anh}(T) + e_{IS}(T), \tag{4}$$

where $E_{harm}(T) = 3nkT$ is the classical mechanical contribution from harmonic vibration about the inherent structure minima and $E_{anh}(T)$ is the anharmonic contribution to the vibration energy. Assuming vibration contributions about any of the inherent structure minima are similar and based on the fact that a the enthalpy follows the DuLong and Petit line very well to high temperatures for our purposes we neglect the anharmonic contributions, whence

$$C_P(T) = (\partial H(T)/\partial T) \approx 3nk + (\partial e_{IS}(T)/\partial T)_P, \tag{5}$$

The configurational contribution to the entropy is

$$S_C(T) = S_C(T_0) + \int_{T_0}^{T} (1/T')(\partial e_{IS}(T')/\partial T')_P \, dT'. \tag{6}$$

where T_0 is a temperature at which $S_C(T)$ is a constant.

In a previous publication[9] a statistical mechanical model was suggested for the contributions to the energy and heat capacity from populating local amorphous minima. This model assumes that a topological lattice can be constructed and that populations of local defect minima on this lattice are responsible for the inherent structures. The configuration part of the partition function can then be written

$$Z_C(T) = \left(\sum_i g_i \exp(-\varepsilon_i / kT) \right)^n . \tag{7}$$

n is the number of sites that may contain defects. ε_i is the minimum potential energy of the ith local defect and g_i is its degeneracy. The partition function in this model is similar to the expression for the partition function contributions for electronic states on a lattice, the difference being that the electronic excited states on each atom or molecule are replaced by defect states on SiO_2 lattice units in the glass. Using Eq. 7 yields a simple expression for the inherent structural contribution to the energy and heat capacity.

$$e_{IS}(T) \approx kT^2 \partial \ln Z_C / \partial T = nkT \sum x_i g_i \exp(-x_i) / \left[\sum g_i \exp(-x_i) \right]$$
$$C_{IS}(T) \approx nk \left[\frac{\sum x_i^2 g_i \exp(-x_i)}{\sum g_i \exp(-x_i)} - \frac{\left[\sum x_i g_i \exp(-x_i) \right]^2}{\left[\sum g_i \exp(-x_i) \right]^2} \right], \quad \text{where } x_i = \varepsilon_i / kT \tag{8}$$

Figure 11 shows a graph illustrating the behavior of the heat capacity using Eq. 8 with some representative values for local potential energy minima. The overall behavior is similar to the heat capacity curves in Figure 5. To fit the MD heat capacity curves would require inherent structural minima at ~ 0.7-1eV for the soft force fields while the strong force fields require minima at ~ 1.3 eV . These are in the range of the energy required to break Si-O bonds shown in Figure 1 (a). As indicated in the previous publications[9] [6], the defects corresponding to these minima are three and five coordinated silicon atoms and non-bridging oxygen atoms. If the definition of a 'fragile' glass is that there is a significant increase in heat capacity of the liquid relative to the solid glass then the MD glasses are fragile glasses at the higher temperatures. For the soft force fields there is an increase in heat capacity relative to the solid of ~ 10 % at 1800 K in agreement with experiment[5]. Experimentally the glass transition occurs below the region of increase in heat capacity and by this definition the glass is behaving as a 'strong' glass.

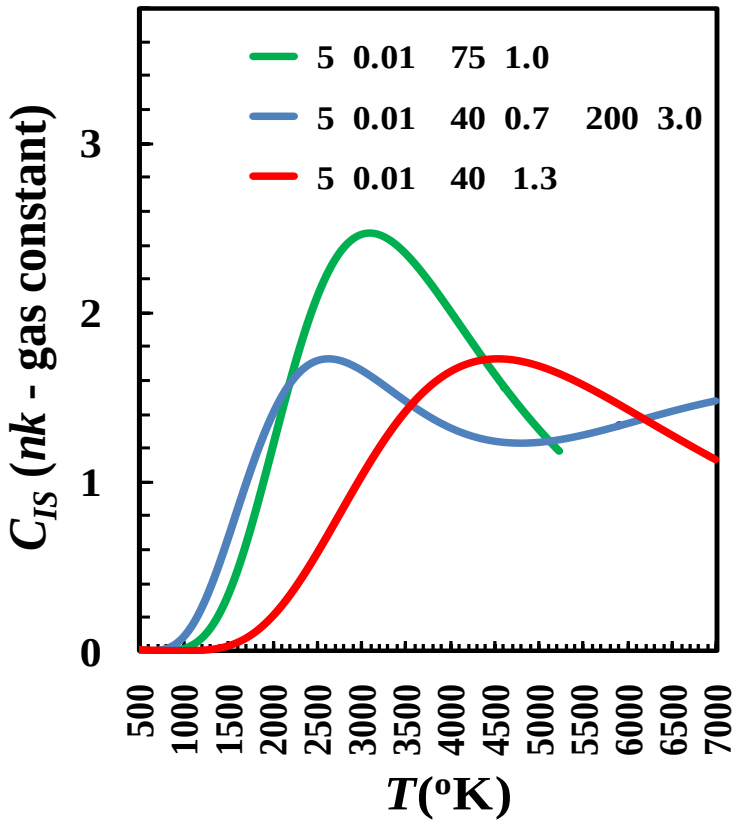

Figure 11 Heat capacity curves generated using Eq. 8 and numbers in the legend that indicating degeneracy and energy in eV of levels. For example the green curve was generated with two local defect energies: one with a degeneracy of 5 at 0.01 eV and the second a degeneracy of 75 at 1.0 eV.

Assuming that topological changes in the ring structure are independent, another partition function with the same form as Eq. 8 might be constructed with low energy transitions. representing different topological ring structures in the glass and this partition function would multiply. However, although transitions involving the breaking and reforming of the ring structure have a high activation energy giving rise to a high activation energy for viscosity there is little net change in energy after the transition and hence these topological reconstructions responsible for glass flow contribute little to the heat capacity.

Below the fictive temperature the term $e_{IS}(T)$ becomes a constant $e_{IS}(T_f)$ where T_f is the fictive temperature and as indicated the heat capacity of the MD simulations becomes ~3 *n k*.

C. Self-diffusion coefficients

The activation energies for self-diffusion for all four potentials investigated here are much less the activation energy for 1/viscosity for silica, namely, ~73 kK (see Figure 10). There is some experimental diffusion data for oxygen self-diffusion in vitreous silica that supports a lower activation energy[39] [40]. This suggests that the Stokes-Einstein relation does not apply to these tetrahedral network glasses. Further the activation energies for diffusion are correlated with the melting temperatures so that if a very strong potential force field is used which does give activation for self-diffusion in the range of the activation energy for viscosity[41] then the predicted melting temperatures and densification temperatures will become even much higher. An effort to decouple the activation energy for diffusion from melting temperatures by devising force fields for which the activation energy for bond breaking shown in Fig. 1 was increased while maintaining a reasonable cohesive enthalpy between 20 and 30 eV[42] were not successful.

V. CONCLUDING REMARKS

While the strong potentials based on *ab-initio* calculations in particular the BKS and CHIK potentials yield many of the properties of the liquid they do so at too high temperatures. The softer force fields proposed by Takada et al. and Demicralp, et al. fit the experimental melting point of β-crytobalite and elastic constants of silica glass but fail to fit the low thermal expansion of solid silica glass and

[39] E. W. Sucov, J. of the Am. Ceram. Soc. 46, 14 (1963).
[40] H. A. Schaeffer, J. of Non-Crys. Solids 38 & 39, 545-550 (1980).
[41] T. F. Soules, J. Non-Cryst. Solids 73, 315-330 (1985)..
[42] F. Liu, S. H. Garofalini, D. King-Smith and D. Vanderbilt, Phys. Rev. B 49, 12528 (1994).

densification. It is possible that a perhaps empirical hybrid force field could fit liquid experimental properties at temperatures that are close to those measured and fit the properties of the solid.

Our results also suggest that a 'strong' glass former defined as one with little change in heat capacity at the glass transition is one in which hopping from one minima to another results in no significant change in potential energy, for example topological changes in the silica ring network by exchanging corner sharing tetrahedral connections. On the other hand at higher temperatures even for these strong glasses high potential energy defect minima come into play and populating these defect states does require the expenditure of energy and hence a structural contribution to the enthalpy and heat capacity.

Important practical results of this study include the fact that relatively short range empirical potentials that are very efficient in MD simulations can be used and appear to be just as accurate as those having longer range Coulombic forces in reproducing certain experimental results.

In a future publication we will refine the pairwise potentials in order to find a single set that faithfully reproduces the experimental properties of liquid and solid vitreous silica and can be used to aid in our understanding of the properties silica under conditions of laser mitigation. Laser mitigation experiments will allow us to explore very fast heating and cooling rates and determine whether fragile liquid behavior can be observed in real silica glass as well as other information including the maximum fictive temperature possible.

Acknowledgments

This work was performed under the auspices of the U. S. Department of Energy by Lawrence Livermore National Laboratory under Contract DE-AC52-07NA27344. The authors would also like to thank Professor Bruce Berne for supplying his potentials.

FIGURE CAPTIONS

Figure 1 Graphs of the radial force fields being compared in this paper. The dashed lines indicate values at the nearest neighbor distances. The numbers labeled E* are activation energies in eV/atom determined as difference in potential energies between the equilibrium positions and the point of inflection in the potential energy curves.

Figure 2 Enthalpy versus temperature during heating of the MD ensembles for the four force fields. Kinks in the curves indicate the homogenous melting temperatures when the MD heating is carried out at ~ 4000 ^{o}K/ns. Insert shows effect of heating rate on the melting temperature with BKS potential. T_m are estimated thermodynamic melting temperatures of the MD ensembles using the methods discussed in the text.

Figure 3 Cross section through a silica MD ensemble in which the atoms of the upper half are held at a temperature below the spontaneous melting temperature and the lower half is heated above the melting temperature. Figure 3 (b) shows a snapshot after allowing the two layers come to an equilibrium temperature. The liquid crystal interface has moved into the crystal region indicating some melting of the crystal. Because the oxygen atoms show more disorder only the silicon atoms are shown.

Figure 4 Simulated MD melting of an ensemble of β-crystobalite (showing Si atoms as blue diamonds) in contact with a melted SiO2 glass (red diamonds) at the same temperature using the CHIK force field and a heating rate of 300 ^{o}K/ns. The potential energy versus temperature of the system is the data with scatter. The smooth curve is the mean squared displacement (MSD) of the crystal atoms versus temperature. Melting is determined by the break in the MSD curve, movement of front of disorder in the lattice and a change in slope of the potential energy.

Figure 5 Enthalpy versus temperature during cooling of MD silica glass runs under NPH conditions at 1000 ^{o}K/ns. T_f , the fictive temperatures, are the temperatures at which the liquid configuration is arrested on the time scale of the cooling indicated by the intersection of extrapolations of the solid and liquid curves.

Figure 6 Heat capacity, C_p, curves obtained by taking the derivative of the enthalpy curves in Figure 4 as discussed in the text.

Figure 7 Sketch illustrating the ring structure of vitreous silica with corner connected tetrahedral. The figure shows the low energy rocking modes of oxygen atoms perpendicular to the axis between silicon atoms.

Figure 8 Density during MD cooling for each of the force fields tested. The numbers in the legend are volumetric thermal contraction coefficients per degree K in the solid temperature range (300-1500 ^{o}K).

Figure 9 The pair radial distribution functions at room temperature from MD cooling simulations. Also shown are the cumulative number of neighboring atoms as a function of distance.

Figure 10 The figure on the left is a sample of the mean square displacements of atoms at different temperatures, in this case Si atoms using the BKS potential. The MD ensemble was cooled to each temperature indicated in the curves and then run for 100 psec. The graphs on the right are diffusion constants obtained from the long time slopes of the mean square displacements.

Figure 11 Heat capacity curves generated using Eq. 8 and numbers in the legend that indicating degeneracy and energy in eV of levels. For example the green curve was generated with two local defect energies: one with a degeneracy of 5 at 0.01 eV and the second a degeneracy of 75 at 1.0 eV.